J. Fluid Mech. (2003), *vol.* 497, *pp.* 225–234.
DOI: 10.1017/S0022112003006827 Printed in the United Kingdom

A circulation description of a rip current neck

By A. B. KENNEDY

Department of Civil & Coastal Engineering, University of Florida, Gainesville, FL 32611-6590, USA

(Received 28 April 2003 and in revised form 29 September 2003)

This paper considers wave-driven rip currents from a circulation–vorticity point of view. A highly simplified description of rip currents using continuous generation of point vortices at fixed locations is found to have a wide range of applicability around the rip neck. Rip scaling becomes straightforward, and is seen to collapse to a single form. Numerical experiments with this simplified system have the ability to predict well startup transients including previously unexplained peaks, and frequency-dependent effects of wave groups on rip currents. Quantitative mean currents in the rip neck are represented moderately well by this theory.

1. Introduction

Wave-driven rip currents are of considerable interest from a scientific viewpoint: their unsteady behaviour on many time scales offers hydrodynamic challenges, while their dependence on, and possible interaction with, bottom sediments means that their hydrodynamics help to shape the topography that drives them in ways which are not completely understood. From a more practical point of view, many people are drowned every year in rip currents, and thus their prediction assumes some importance.

Shepard, Emery & La Fond (1941) provided a basic description of rip currents that persists to this day: shore-parallel feeder currents join at a rip neck and become a narrow, offshore directed rip current that persists for several surf zone widths. A more gentle return flow brings water back into the surf zone. Numerous other field investigators have confirmed these basic descriptions and mapped circulation, typical strengths, and persistence.

On the basis of work by Longuet-Higgins & Stewart (1964) and others on wave-induced radiation stresses, it became possible to predict numerically rip current evolution over longshore-varying topographies using wave phase-averaged techniques. This has prompted a variety of numerical studies of various aspects of rip current evolution (Ebersole & Dalrymple 1980; Haas, Svendsen & Haller 1998), which have provided numerous insights into rip current behaviour.

However, in radiation stress descriptions of rip currents, irrotational and rotational forcing are intertwined in a complex manner. It is notable that there are no simplified descriptions of rip currents which may be used to provide estimates of strength and temporal variation for both scientific description and practical purposes. We will address this problem here.

2. Simplified representation of rip currents

A defining feature of topographically controlled rip currents is that the locations of wave breaking are more or less stationary on hydrodynamic scales. This leads to

strong wave breaking on a bar or shore-connected shoal, and weak or no breaking in the rip channel.

As shown by Peregrine (1998), whenever the strength of breaking in shallow water varies along a wave crest, this generates circulation, defined as $\Gamma \equiv \oint \boldsymbol{U} \cdot \mathrm{d}l$. (See also Bühler & Jacobson 2001 for background on wave breaking and vorticity.) For rip currents, most or all circulation will be generated in the vicinity of the rip channel, where breaking varies in the longshore coordinate from strong to weak in a short distance. Because oppositely signed circulation is generated on either side of the rip channel, mutual advection between the two sides transports vorticity offshore. Circulation continues to be generated at fixed locations on either side of the rip current. This is quite similar to the conceptual representation of Peregrine (1999), who described an offshore-propagating vortex couple resulting from short gaps in breaking waves.

This is also the essence of our description: *in the area of the rip neck, the dynamics of a rip current can be represented by continuously generated circulation at fixed locations on either side of the rip channel.* In its simplest form, which we will use here, there are only two independent parameters: the half-width of the rip channel, R, and the mean rate of generation of circulation, $(\mathrm{D}\Gamma/\mathrm{D}t)_0$, which is forced by wave breaking. All variables then scale accordingly as a dimensionless group:

$$(x^*, y^*) = (x, y)/R, \quad t^* = t(\mathrm{D}\Gamma/\mathrm{D}t)_0^{1/2}/R,$$
$$(u^*, v^*) = (u, v)/(\mathrm{D}\Gamma/\mathrm{D}t)_0^{1/2}, \quad \Gamma^* = \Gamma/\left(R(\mathrm{D}\Gamma/\mathrm{D}t)_0^{1/2}\right).$$

Because in this simple representation we assume shallow water and a locally flat bed, there is no third dimension. Such a description encompasses major aspects of rip currents: strong offshore velocities in the rip channel, and a weaker return flow. As will be seen in numerical experiments, even growing jet instabilities are seen.

There are immediate benefits: time in rip currents scales with $R/(\mathrm{D}\Gamma/\mathrm{D}t)_0^{1/2}$, and thus the temporal response varies with both the length scales of the system and the strength of wave breaking. Although rip currents have long been observed to vary with wave group forcing, no simple dynamical description of this phenomenon has ever been given. Similarly, velocities in the rip channel scale with $(\mathrm{D}\Gamma/\mathrm{D}t)_0^{1/2}$, and are independent of the gap width. Again, independent of this, there has been no good way to scale velocities in the rip channel.

It is easy to find omissions in this simple description of dynamics in the rip neck. Certainly, these will affect some quantitative aspects of the system, but for a system which looks like a rip current, they appear to have a relatively weak effect on dynamics. However, offshore of the rip neck, and at other areas in the circulation cell, this description is certainly lacking.

2.1. *Numerical description*

An analytical description of this system including unsteady effects does not appear to be feasible, so we examine the reduced system numerically using a discrete vortex method. All quantities from now on are dimensionless unless stated otherwise, but with no asterisks for simplicity.

Using the relation for point vortex velocities, $U_\theta = \Gamma/2\pi r$, where r is the radial distance from a vortex, we compute the velocity, $\boldsymbol{U}$, at some vortex as the sum of that induced by all other vortices in the domain. The location of each vortex is then advanced in time using a simple Euler method $(X, Y)^{(t+\delta t)} = (X, Y)^{(t)} + \boldsymbol{U}\delta t$.

New point vortices of opposite sign were introduced into the system at $(x, y) = (0, \pm 1)$, at intervals Δt. Note that new vortices were not introduced at the small time

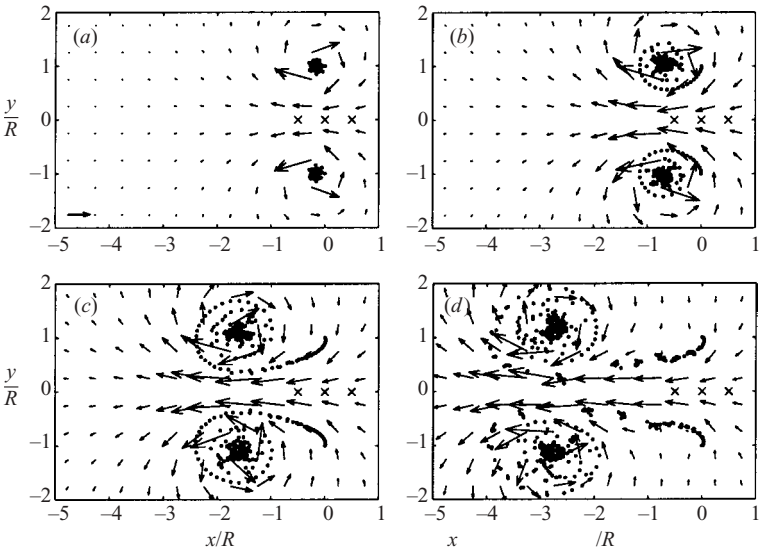

FIGURE 1. Startup in a simplified rip current system starting at dimensionless time 2.5 and with 2.5 interval between snapshots. The vector at bottom left of (*a*) has magnitude 1. ·, point vortices; ×, location along centreline where results are to be presented.

step, δt, but rather at a large time step, $\Delta t = N\delta t$, where $20 \leqslant N \leqslant 125$. This separation of scales was necessary because of the strong interactions between consecutively introduced point vortices, which had very small separation. To allow sinuous instabilities to form, random perturbations of relative magnitude 10^{-5} were added to each vortex as it was introduced.

This method is quite simplistic, and it would require much care to examine growth of the resulting jet offshore. However, for steady forcing, behaviour in the vicinity of the rip neck is much simpler with generally small fluctuations. Convergence tests indicate good accuracy: for steady forcing, mean velocities presented here are within 0.1% relative. Results for unsteady forcing are more challenging to quantify because of subharmonic and chaotic response at some forcing frequencies. At the midpoint between the two sources of circulation, convergence tests indicate that RMS accuracy for velocity fluctuations is around 2% averaged over a wide range of frequencies, with greatest errors for higher frequency forcing. Any error in the numerical results is an order of magnitude smaller than would be found, for example, in determining field-scale geometries or in neglected processes.

2.2. *Startup velocities*

Very large, repeatable, velocity peaks have been observed experimentally in the rip neck during startup (Kennedy & Dalrymple 2001). These are of interest, as pulses generated by wave groups may be one of the most important factors in evaluating rip current safety.

Figure 1 shows computations of our simplified system from startup using constant forcing. Each point in the figure represents one of the point vortices, so their density is a measure of vorticity in real-world systems. The sequence shows a vortex couple which first grows in the area where it is generated, then as it continues to increase in strength, detaches and advects offshore. After this, its behaviour in the vicinity of the rip neck resembles a jet more than the vortex couple seen immediately at startup.

This is in accordance with more complete numerical computations, which have also predicted strong vortex generation at bar corners, and subsequent mutual advection offshore (Chen *et al.* 1999). Such qualitative agreement is welcome, though not unexpected.

For quantitative comparisons of the simplified description, we compare with laboratory experiments of Kennedy & Dalrymple (2001), and additional data not reported in that study. These experiments were performed on the setup of Haller, Dalrymple & Svendsen (2002), which is a barred beach topography bisected by two rip channels. Three synoptic acoustic Doppler velocimeter (ADV) measurements were made at the centreline of the right rip channel and 20 cm to either side, at a cross-shore position of $x = 11.8$ m. Surface elevation data were also taken offshore. For examining startup conditions, we will only use records with monochromatic waves, but later tests will also include unsteady bichromatic forcing.

Measured time series of cross-shore velocities will be used to test the simplified system. Because of turbulent instabilities at times when there was also a strong temporal variation in the mean signal, velocities at the three ADVs were averaged into one record. Measured velocities were also converted to depth-averaged mass-transport velocities, using records at the three ADVs and small-amplitude wave theory to estimate time series of wave heights and Doppler shifts. This was necessary as the simplified system is written in terms of mass-transport velocity. Experimental velocities and times were scaled using R and $(\mathrm{D}\Gamma/\mathrm{D}t)_0$ for comparison with the simplified model. R is easily seen to be around 0.9 m, but estimates of $\mathrm{D}\Gamma/\mathrm{D}t$ are somewhat more difficult.

However, Brocchini *et al.* (2003) and Kennedy *et al.* (2003), considered the problem of circulation generation on topographies where waves broke on a bar but not in a rip channel. The estimate which appeared most reasonable was for waves which broke on a slope according to $(H/h)_{max} = \gamma$ and then continued to break on the flat bar crest, ending with height $(H/h_c) = \beta$. This gave an estimate of circulation generation:

$$\frac{\mathrm{D}\Gamma}{\mathrm{D}t} = \frac{5g\gamma^2}{16}(h_B - h_c) + \frac{gh_c}{8}(\gamma^2 - \beta^2), \quad \frac{\mathrm{D}\Gamma}{\mathrm{D}t} \geqslant 0, \tag{2.1}$$

where $\gamma = 0.78$ and $\beta = 0.45$ are relatively standard constants. The breaking depth, h_B, was estimated as

$$h_B = \left(H_0^2 C_{g0}\right)^{2/5} \gamma^{-4/5} g^{-1/5}, \tag{2.2}$$

where H_0 and C_{g0} are the wave height and group velocity at some point offshore of the bar. For monochromatic wave forcing, H_0 and thus $\mathrm{D}\Gamma/\mathrm{D}t$ were constant in time. For bichromatic tests to come, with wave frequencies ω_1, ω_2, wave height varied with group frequency $\omega = |\omega_1 - \omega_2|$, and generation of circulation and velocity response are also unsteady. In these cases, $(\mathrm{D}\Gamma/\mathrm{D}t)_0$ is the mean forcing over time.

Using these estimates, measured velocity records could then be scaled. Figure 2 shows time series from the simplified system. Velocity traces are shown at three locations along the centreline as it is somewhat difficult to know exactly where the laboratory measurements were taken in relation to the location of circulation generation. Overlying this are means and standard deviations of scaled records from the laboratory tests.

Strong similarities are seen between the simplified system and laboratory measurements. In each, velocity rises quickly, reaches a peak, and then declines to a lower value. The instant and magnitude of peak velocity varies with cross-shore position in the simplified system with a later and larger peak further offshore. This

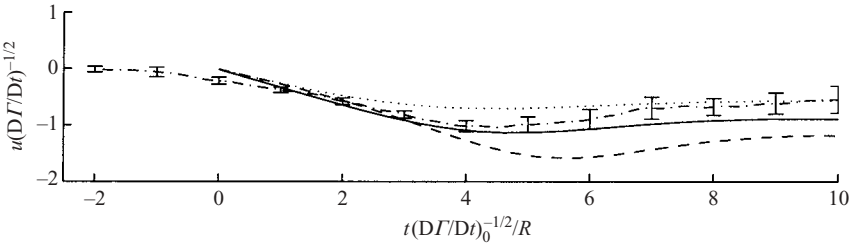

FIGURE 2. Centreline velocities in a rip current system at startup. Simplified system: —, $(x, y) = (0, 0)$; ——, $(x, y) = (-0.5, 0)$; ···, $(x, y) = (0.5, 0)$. —·—, Mean of six scaled laboratory tests; error bars give $\pm$ one standard deviation.

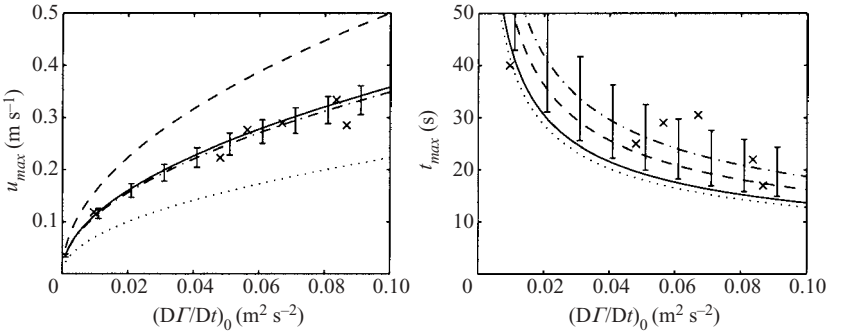

FIGURE 3. Measured peak velocities and times to peak at startup. ×, Experimental measurements. Simplified system: —, $(x, y) = (0, 0)$; ——, $(x, y) = (-0.5, 0)$; ···, $(x, y) = (0.5, 0)$. —·—, $u_{max} = C_1\sqrt{D\Gamma/Dt}$, and $t_{max} = C_2 R/\sqrt{D\Gamma/Dt}$ with C_1 and C_2 calculated from laboratory measurements. Error bars show $\pm$ one standard deviation on C_1 and C_2.

corresponds well to the sequence shown in figure 1, and the decline in velocity after the peak is then due to the ejection of the initial vortex.

The laboratory results correspond well to the simplified system at $(x, y) = (0, 0)$, midway between the locations of circulation generation. However, experimental measurements show a considerably larger decline in velocity after the peak, which may be due to the beginnings of wave–current interaction, or to other factors. The standard deviation of scaled laboratory measurements is relatively small considering the wide range of wave conditions.

Figure 3 shows dimensional measurements of peak startup velocities and times to the peak for a greater number of tests. Time to peak velocity involves some judgement, as the laboratory wavemaker had a ramp-up time during which wave heights were smaller than specified. Dimensional estimates of peak velocities and times to peak for the simplified system, both using $R = 0.9$ m, are plotted for comparison.

Peak velocities agree very well with results from the simplified system at $(x, y) = (0, 0)$. Predicted times to peak velocity are generally underestimated, but still reasonable for such a simple estimate. Differences may partly stem from uncertainties in starting times, but are large enough that effects of neglected processes are probably significant. However, overall agreement at startup seems to bolster the simplified description considerably.

Finally, we note that two startup tests with monochromatic waves were excluded from figures 2 and 3. In these, flow quickly became very turbulent and it proved

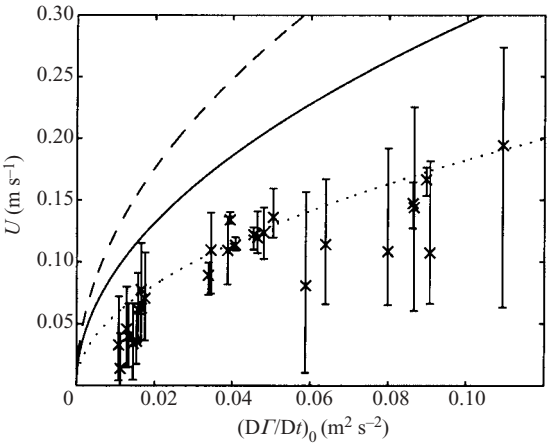

FIGURE 4. Mean velocities in the rip neck. Simplified model: —, $(x, y) = (0, 0)$; ——, $(x, y) = (-0.5, 0)$; ···, $(x, y) = (0.5, 0)$. Laboratory measurements: ×, mean over the three ADVs. Error bars show the highest and lowest mean from the three ADVs.

impossible to determine either a peak velocity or time to peak. As these tests had a considerably lower ratio of water depths over the bar and channel than other tests (1:3.5), it may prove to be a limit of the simplified theory, although more work is needed. However, these two tests are included in mean velocity comparisons, and do not appear out of line with other measurements.

2.3. *Mean velocities in the rip neck*

An examination of figure 2 shows that, in the simplified system, centreline velocities asymptote to near-constant values at the measurement locations along the centreline. This is not strictly true: instabilities cause the velocity to vary, but at the locations considered, these are small. Further offshore, instabilities grow very quickly, and large coherent structures form that appear in many ways like the shallower jets in Dracos, Giger & Jirka (1992); however, this leads into a very different topic that will not be explored here. For the case of rip currents, the simplified representation is limited to the immediate vicinity of the rip channel.

For the experimental system, currents in the rip neck are not steady, even for monochromatic wave forcing, which has been attributed to a jet instability of the rip current (Haller & Dalrymple 2001), and can be significant. However, averaged over a sufficiently long interval, highly repeatable values may be found. Applicability of the simplified representation to such a complex situation thus seems somewhat uncertain, but reasonable agreement with experiments may still be found.

Figure 4 shows dimensional mean velocities for a large number of experimental tests, compared to results from the simplified representation. Experimental results here also include tests with bichromatic forcing which were not used when examining startup velocities, as the instantaneous phase of the bichromatic wave group would have been a major complicating factor. As there could be a considerable difference in mean velocities even for ADVs separated by a small distance, the largest and smallest mean of the three ADVs, as well as the mean of all three, are both plotted.

The trend of velocities is very well predicted over a range of forcing with different wave heights, periods, and water levels. However, magnitudes of mean velocity appear to be less than predicted by the simplified system at $(x, y) = (0, 0)$, where good

agreement was found previously for startup peak velocities. Mean velocities over the three ADVs are generally even less than the simplified system at $(x, y) = (0.5, 0)$.

There are many possible reasons for this variation: previously noted flow instabilities are quite strong in this geometry and can cause significant velocity fluctuations over long periods. A further possibility is the flow bias found in many of the tests, where the rip current was significantly skewed to the left or right of the rip channel. Topographic three-dimensionality and the shoreline influence may also be significant here.

2.4. *Response to periodic forcing*

All field reports of rip currents note that they are highly unsteady. This may be partly due to a jet instability, but there have been numerous field observations (Shepard *et al.*, 1941; and many others) and some laboratory experiments (Kennedy & Dalrymple 2001) linking rip current pulsations to short-wave groups. Anecdotal evidence also links these pulsations to swimmer distress: venturing into rips during periods of lower current, they are swept offshore when the current rises. Further empirical evidence suggests that rip currents are most dangerous when longer period waves are incident (Lascody 1998).

The connection between wave groups and rip current pulsations is undeniable, but until now, there has been no good way to link the two, or even to scale them. However, with the proposed scaling, this becomes simple. Using $u \propto (\mathrm{D}\Gamma/\mathrm{D}t)^{1/2}$ and tangent linearity leads to the non-dimensional velocity fluctuation $\Delta u^* = \Delta u(\mathrm{D}\Gamma/\mathrm{D}t)_0^{1/2}/\Delta(\mathrm{D}\Gamma/\mathrm{D}t)$. The non-dimensional wave group frequency for a bichromatic wave train is then $\omega^* = \omega R/(\mathrm{D}\Gamma/\mathrm{D}t)_0^{1/2}$. This frequency scaling is of considerable importance as it again makes explicit that the response time scales of a rip current system depend not only on the geometry, but also on the strength of forcing. This is in direct opposition to gravity wave Froude number scaling, where time scales do not vary with forcing strength.

To test these scalings, the steady forcing of the previous section was replaced with a harmonic representation of arbitrary period and amplitude, and a mean of unity:

$$\frac{\mathrm{D}\Gamma}{\mathrm{D}t} = 1 + a\sin(\omega t). \tag{2.3}$$

For a first test, the amplitude was set to $a = 1$, and the forcing frequency varied – computations using other values of a had quantitative differences, but identical trends. The velocity along along the centreline was recorded and the fluctuating amplitude computed as $\Delta u = 2^{1/2}\sigma_u$, using σ as the standard deviation operator, working again in dimensionless variables, and capturing an integer number of forcing periods. For some of the higher frequencies, the response became partially subharmonic or chaotic and some finite sample length error may be introduced, but this is likely to be small in comparison to other factors.

Some limiting results may be found for both high and low frequencies. For low frequencies, velocities are in instantaneous equilibrium with forcing, and solutions may be found analytically for the case $a = 1$. The mean velocity becomes $\overline{u} = \overline{u}_m 8^{1/2}/\pi$, where $\overline{u}_m$ is the mean velocity at any location for steady forcing with the same mean $\mathrm{D}\Gamma/\mathrm{D}t$. Thus, the mean velocity is around 10% lower for highly unsteady low-frequency forcing. This may have been a contributing factor to the low laboratory velocities noted in figure 4 where many of the bichromatic tests were highly unsteady. The amplitude of the low-frequency velocity fluctuation is found to be $\Delta u = \overline{u_m} 2^{1/2}(1 - 8/\pi^2)^{1/2}$.

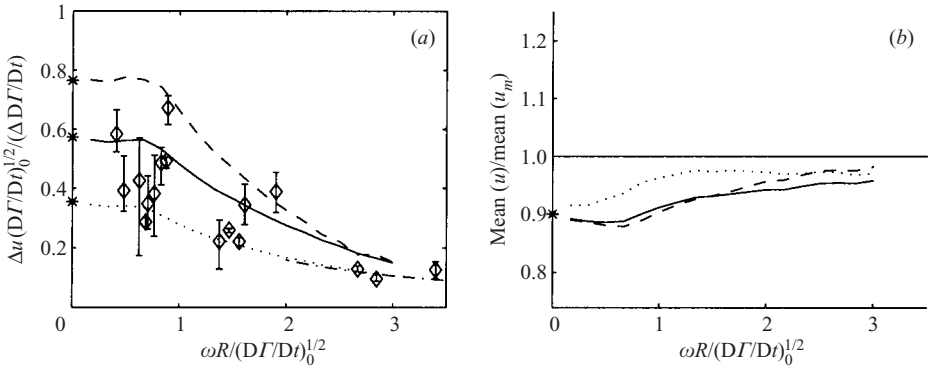

FIGURE 5. Rip current response to time-varying forcing. (a) Amplitude of velocity fluctuations; (b) mean velocity relative to steady forcing. Simplified model, $a = 1$: —, $(x, y) = (0, 0)$; ——, $(x, y) = (-0.5, 0)$; ···, $(x, y) = (0.5, 0)$. *, Low-frequency limits; —•—, high-frequency limit at $(x, y) = (0, 0)$. ◇, Laboratory measurements. Error bars show the highest and lowest amplitudes over the three ADVs.

For high frequencies, we may also make analytical approximations, assuming that both growing instabilities and restoring forces are small on this scale. The amplitude of the fluctuation at any location along the centreline is then $\Delta u = \Delta \mathrm{D}\Gamma/\mathrm{D}t/(\pi\omega(1+y^2))$.

For the laboratory experiments, fluctuations were computed as $\Delta \mathrm{D}\Gamma/\mathrm{D}t = 2^{1/2}\sigma_{\mathrm{D}\Gamma/\mathrm{D}t}$ and $\Delta u = 2^{1/2}\sigma_u$, where velocity measurements were first band-pass filtered about the group frequency to minimize the effects of jet instabilities. Figure 5 plots laboratory data with results from the simplified system. Measured velocity fluctuations tend to be over the low range of the theoretical system, but are still quite reasonable. Experimental results often showed very pronounced, extremely low-frequency (many group periods) amplitude modulation, which may contribute to the differences. For both data sets, a drop-off in velocity response with increasing frequency is both obvious and significant.

The ramifications of a frequency-varying response are considerable, making it useful to pursue dimensional examples. A typical value for the half-width of a field-scale rip current might be 15 m, while generation of circulation might be $1\,\mathrm{m}^2\,\mathrm{s}^{-2}$. For frequencies of $\omega R/(\mathrm{D}\Gamma/\mathrm{D}t)_0^{1/2} > 1$, figure 5 shows that the response decreases quickly. Converting this to dimensional quantities gives the result that for group periods greater than $T_{group} \approx 100$ s, there will be a strong response at the forcing frequency, while for shorter group periods, there will be much less response. Thus, for any wave conditions with this mean forcing, the unsteady response will depend on the spectrum of unsteady forcing.

Now consider wave trains with this mean forcing, but different peak frequencies: a narrow-banded swell with peak period $T_p = 12$ s, and a broad-banded sea with $T_p = 6$ s. The 12 s swell will have much greater forcing for $T_{group} > 100$ s when compared to the 6 s sea. Thus, rip currents under the swell conditions will have stronger pulsations than with the sea conditions. This provides physically based justification for the empirical evidence that rip currents can be more dangerous under long-period swell forcing.

3. Discussion and limitations

Given the great complexity of physical rip currents, it is somewhat surprising that the simplified system works at all. Of neglected processes, wave–current interaction,

three-dimensional topography, bottom friction, shore vortices, forced and free low-frequency gravity waves, and instabilities can all be significant. We believe that the reason for the success of this description is that, in the area of the rip neck, the interaction between oppositely signed circulation on either side of the rip neck is the overwhelming process. Other processes will modify this, but will not change its general nature. In situations where these other processes are comparable in strength to vortex-couple mutual advection, this model will show increasing errors. (See Brocchini *et al.* 2003 and Kennedy *et al.* 2003 for a detailed discussion of other factors affecting initial vortex transport.) Away from the rip neck, the model breaks down quickly – other processes which are not included here will dominate.

For any estimate of rip current properties, $D\Gamma/Dt$ must also be estimated. This depends strongly on details of local topography, which may be difficult to determine *a priori*. For known geometries, (2.1)–(2.2) give estimates of $D\Gamma/Dt$ for the specific conditions of wave breaking on gently sloping, wide-crested bars or breakwaters with shore-normal waves that do not break in the rip channel. However, their general applicability is not yet demonstrated.

Further challenges include the field determination of x/R, the cross-shore location of circulation generation. This may change somewhat with wave height and tidal level, and may be spread over a significant distance. Again, this will affect quantitative descriptions.

Finally, all laboratory data used here came from a single topography (Haller & Dalrymple 2002). Although many different combinations of wave height, period, water level, and unsteadiness were used, additional data from other sites would be useful.

4. Conclusions

Based on the results presented here, we make some conclusions.

(*a*) Time in the neck of rip current systems scales like $t^* = t(D\Gamma/Dt)_0^{1/2}/R$, and horizontal velocities scale like $(u^*, v^*) = (u, v)(D\Gamma/Dt)_0^{-1/2}$. Using this scaling, all rip current topographies collapse to a single form,

(*b*) The simplified rip current description presented here predicts rip current startup velocities quantitatively quite well startup time scales reasonably well; mean velocities moderately well, and response to unsteady wave forcing quite well,

(*c*) Large velocities observed in the rip neck at startup are due to a strong initial vortex couple that grows in the rip neck. A decrease in velocity is then seen when the vortex couple migrates offshore,

(*d*) Rip current response to unsteady wave forcing is strongly dependent on the wave group forcing frequency. The response is greatest for dimensionless frequencies $\omega R/(D\Gamma/Dt)_0^{1/2} \leqslant 1$, and decreases quickly for higher frequencies.

A. B. K. was supported in this work by the University of Florida.

REFERENCES

Brocchini, M., Kennedy, A. B., Soldini, L. & Mancinelli, A. 2003 Topographically-controlled, breaking wave-induced macrovortices. Part 1. Widely separated breakwaters. *J. Fluid Mech.* (submitted).

Bühler, O. & Jacobson, T. E. 2001 Wave-driven currents and vortex dynamics on barred beaches. *J. Fluid Mech.* **449**, 313–339.

Chen, Q., Kirby, J. T., Dalrymple, R. A., Kennedy, A. B. & Haller, M. C. 1999 Boussinesq modelling of a rip current system. *J. Geophys. Res.* **104**, 20617–20637.

Dracos, T., Giger, M. & Jirka, G. H. 1992 Plane turbulent jets in a bounded fluid layer. *J. Fluid Mech.* **241**, 587–614.

Ebersole, B. A. & Dalrymple, R. A. 1980 Numerical modelling of nearshore circulation. *17th Intl Conf. Coastal Engng Sydney* (ed. B. L. Edge), pp. 2710–2725. ASCE.

Haas, K. A. & Svendsen, I. A. 2002 Laboratory measurements of the vertical structure of rip currents. *J. Geophys. Res.* **107**, 10.1029/2001JC000911.

Haas, K. A., Svendsen, I. A. & Haller, M. C. 1998 Numerical modelling of nearshore circulation on a barred beach with a rip current. *Proc. 26th Intl Conf. on Coast. Engng – ASCE* vol. 1 (ed. B. L. Edge), pp. 801–814.

Haller, M. C. & Dalrymple, R. A. 2001 Rip current instabilities. *J. Fluid Mech.* **433**, 161–192.

Haller, M. C., Dalrymple, R. A. & Svendsen, I. A. 2002 Experimental study of nearshore dynamics on a barred beach with rip channels. *J. Geophys. Res.* **107**, 10.1029/2001JC000955.

Kennedy, A. B., Brocchini, M., Soldini, L. & Thomas, D. 2003 Topographically-controlled, breaking wave-induced macrovortices. Part 2. Rip current topographies. *J. Fluid Mech.* (submitted).

Kennedy, A. B. & Dalrymple, R. A. 2001 Wave group forcing of rip currents. *Proc. Waves 2001: Ocean Wave Measurement and Analysis – ASCE* vol. 1 (ed. B. L. Edge & J. M. Hemsley), pp. 1426–1435.

Lascody, L. L. 1998 East central Florida rip current program. *Natl Wea. Dig.* **22**, 25–30.

Longuet-Higgins, M. S. & Stewart, R. W. 1964 Radiation stresses in water waves; a physical discussion, with applications. *Deep-Sea Res.* **11**, 529–562.

Peregrine, D. H. 1998 Surf zone currents. *Theor. Comput. Fluid Dyn.* **10**, 295–309.

Peregrine, D. H. 1999 Large-scale vorticity generation by breakers in shallow and deep water. *Eur. J. Mech.* B/*Fluids* **18**, 403–408.

Shepard, F. P., Emery, K. O. & La Fond, E. C. 1941 Rip currents: a process of geological importance. *Trans. Am. Geophys. Union* **31**, 555–565.